Electr Eng (2010) 92:245–255
DOI 10.1007/s00202-010-0182-2

ORIGINAL PAPER

Direct torque control of induction motor based on advanced discontinuous PWM algorithm for reduced current ripple

K. Sri Gowri · T. Brahmananda Reddy · Ch. Sai Babu

Received: 26 June 2009 / Accepted: 3 October 2010 / Published online: 16 October 2010

Abstract In recent years several discontinuous pulse width modulation (DPWM) methods are reported to improve the performance of AC drives at high modulation indices. It is proved that the performance of the popular PWM methods is modulation index dependent and no single DPWM method provides satisfactory performance over the entire high modulation range. Two popular existing DPWM methods renowned with the names DPWMMIN, DPWMMAX clamp each phase for 120° duration in every cycle of its fundamental voltage. It is observed that only the zero state is different in these two sequences. In this paper, it is proposed that, utilizing these two DPWM sequences and by changing the zero state at any spatial angle γ, where γ is between 0° and 60°, an infinite number of DPWM sequences including the existing DPWM methods and advanced DPWM (ADPWM) methods can be generated which are categorized as "continual clamping" and "split clamping" sequences. Using these ADPWM techniques an optimal split clamping sequence-based DTC of induction motor is proposed. With the proposed DTC method it is shown that steady state line current distortionat higher line side voltages is reduced significantly compared with the CDTC as well as conventional SVPWM (CSVPWM)-based DTC.

Keywords Advanced DPWM techniques · CDTC · CSVPWM · Continual clamping · DPWM · HDF · Split clamping · Space vector approach

K. Sri Gowri (✉)
Department of EEE, RGM College of Engineering and Technology, Nandyal 518501, India
e-mail: gowrivasu.3@gmail.com

T. B. Reddy
Department of EEE, G. Pulla Reddy Engineering College, Kurnool, India
e-mail: tbnr@rediffmail.com

Ch. Sai Babu
Department of EEE, JNTU College of Engineering, Kakinada, India
e-mail: chs_eee@yahoo.com

1 Introduction

Research interest in high performance control strategies received researcher's attention extensively over the last three decades. This become speedy after the invention of field oriented control (FOC) by Blaschke [1]. To overcome the complexities involved in FOC-like reference frame transformation, motor parameter dependency, a new control strategy renowned as direct torque control (DTC) was developed by Takahashi [2]. Though conventional DTC (CDTC) is simple, easy to implement generates substantial steady state ripples in torque and flux and acoustical noise. Also, with CDTC the switching frequency is not maintained constant [2,3]. In recent years several PWM techniques were developed to reduce the steady state ripple and to get the constant switching frequency [4,5]. In applications such as inverter fed drives PWM technique employed determines the dc bus utilization, quality of the line current waveforms and inverter switching losses [4,5]. CSVPWM results in higher line side voltage and less line current harmonic distortion than sin-triangle PWM [6–8] with constant switching frequency. Though CSVPWM-based DTC could eliminate some tribulations that are with the CDTC, such as steady state ripples in torque and flux, variable switching frequency, etc., [9–11], at higher line side voltages compared with CSVPWM method, DPWM methods results in reduced line current distortion for a given switching frequency of the inverter [12–16]. Though

theoretically an infinite number of ADPWM methods can be generated, the performance and viability constraints of practical PWM-VSI drives reduce the possibility to a limited number [17,18]. This paper focuses on the generation of both existing DPWM methods and ADPWM methods. Also, few ADPWM methods are analyzed in terms of the harmonic distortion of the line current using space vector approach and finally an optimal ADPWM method which gives least distortion is determined and an optimal ADPWM-based DTC induction motor is proposed particularly for the drive operating at high speeds. With the proposed method it is proved that line current distortion at higher line side voltages is reduced significantly compared with the CDTC as well as conventional SVPWM-based DTC.

2 Proposed DPWM switching sequences

2.1 A SVPWM-based switching sequences

With a three-phase voltage source inverter (VSI) there are eight possible switching states. The two states, from which no power gets transferred from source to load, are termed as null vectors or zero states. The other six states called active states. The active states can be represented by space vectors given in (1) and divides the space vector plane into six equal sectors as shown in Fig. 1. It can be shown that all the six active states can be represented by space vectors given by (1) forming a regular hexagon and dividing it into six equal sectors denoted as I, II, III, IV, V, and VI as shown in Fig. 1.

$$V_k = \frac{2}{3} V_{dc} \times e^{j(k-1)\frac{\pi}{3}}, \quad k = 1, 2, \ldots, 6. \tag{1}$$

In the SVPWM strategy, the desired reference voltage vector is generated by time averaging the two nearby active voltage states and two zero states in every carrier cycle T_s. For a given reference voltage V_{REF} at an angle α with reference to V_1 in first sector, the volt–time balance is maintained

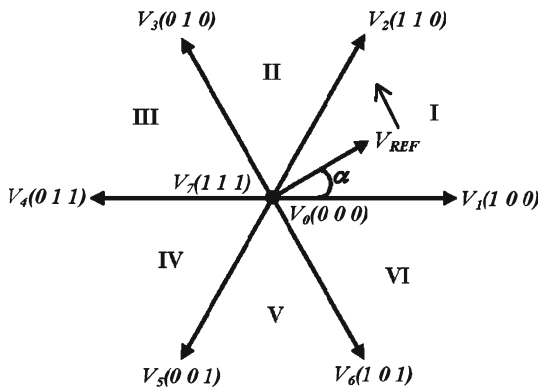

Fig. 1 Switching states and corresponding voltage vectors of a three-phase VSI converter: I, II, III, IV, V, VI are the sectors

by applying the active state1 V_1, active state 2 V_2 and two zero states V_0 and V_7 together for durations, T_1, T_2 and T_Z, respectively, as given in (2.1) [6,7,16–18].

$$T_1 = M \times \frac{\mathrm{Sin}(60^\circ - \alpha)}{\mathrm{Sin}60^\circ} \times T_s \tag{2.1}$$

$$T_2 = M \times \frac{\mathrm{Sin}\alpha}{\mathrm{Sin}60^\circ} \times T_s \tag{2.2}$$

$$T_Z = T_s - T_1 - T_2, \tag{2.3}$$

where 'M' is the modulation index, given by $\mathrm{M} = \frac{3V_{\mathrm{REF}}}{2V_{dc}}$. Although in CSVPWM strategy the two active vectors and two zero vectors must be applied for durations as in (2.1), these can be applied in different ways in different sequences. In [12,15], by varying a single constant variable a generalized DPWM algorithm utilizing the freedom of dividing the zero state time within a sampling period is used to generate different DPWM methods. A zero voltage vector distribution variable σ that divides the zero state time between two zero states are given by (3.1, 3.2).

$$T_0 = T_Z \sigma \tag{3.1}$$

$$T_7 = T_Z\,(1 - \sigma). \tag{3.2}$$

With $\sigma = 1$ DPWMMIN with 012, 210, ... in the first sector and 032, 230, ... in the second sector and so on will be executed and with $\sigma = 0$ DPWMMAX with 721, 127, ... in the first sector and 723, 327, ... in the second sector and so on will be executed. Now onwards these two sequences will be referred in terms of the constant variable σ. These two DPWM sequences, i.e. with $\sigma = 1$ and $\sigma = 0$ uses the zero vectors V_0 and V_7, respectively, for the entire T_Z duration.

Summarizing this, the zero vector can be applied either using V_0 or V_7. CSVPWM uses both for an equal duration of $\frac{T_Z}{2}$, whereas DPWM sequences uses only one of these two for the entire T_Z duration and this results in the clamping of a phase to one of the two buses.

2.2 Existing and advanced DPWM methods

The modulating waveforms of some popular existing DPWM methods are shown in the Fig. 2. The considered DPWM methods are DPWMMAX, DPWMMIN, DPWM0, DPWM1, DPWM2, and DPWM3 [11,12]. These can be generated by properly choosing the zero vectors and the period for which the zero vector/vectors are applied. So, change in the zero state and/or change in the period of application of the zero state results in different DPWM techniques. In this paper, based on the nature of clamping, the DPWM sequences are categorized into two groups: "continual" and "split clamping" sequences. A popular DPWM method clamps every phase during the middle 120° duration for every 360° of fundamental voltage. It is popularly called by the name DPWMMIN. Another well-known method clamps every phase for 60° at the start and at the end for every 360°

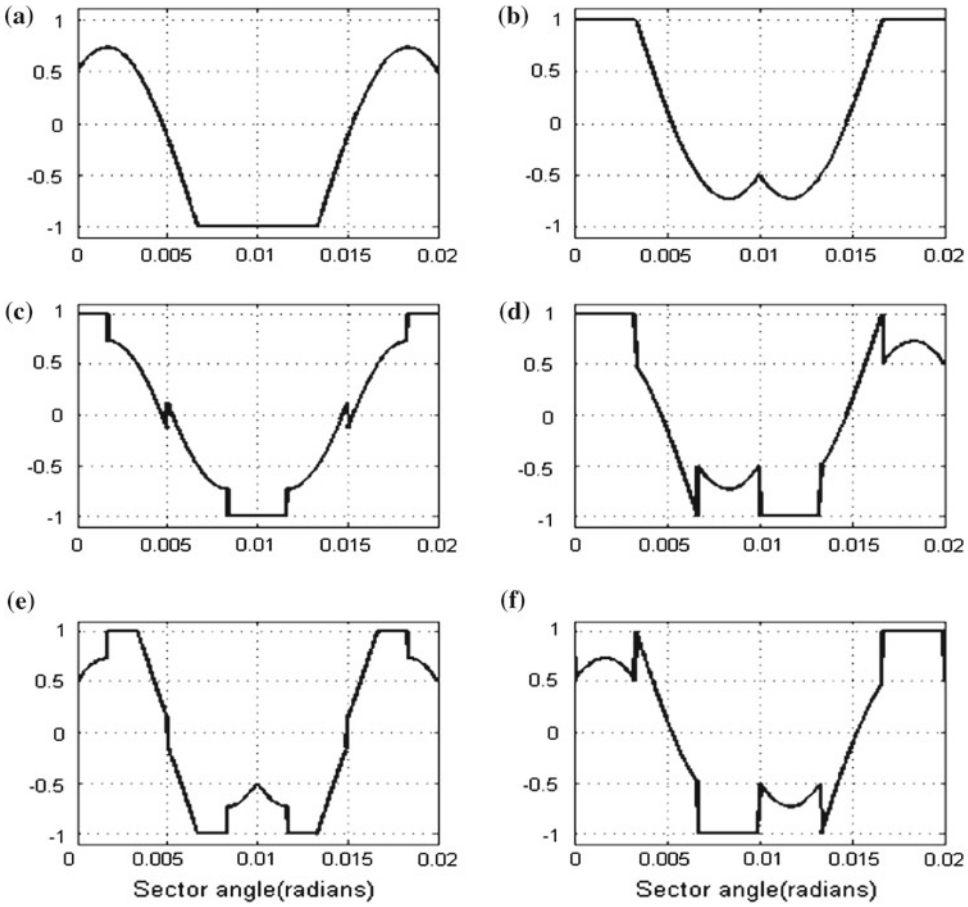

Fig. 2 Modulation waveforms of some popular existing DPWM methods. **a**, **b** Continual or split clamping sequence with $\gamma = 60°$ or $\gamma = 0°$ (DPWMMIN, DPWMMAX), **c** continual clamping sequence with $\gamma = 30°$ (DPWM1), **d** DPWM2, **e** split clamping sequence with $\gamma = 30°$ (DPWM3) and **f** DPWM0

of its fundamental voltage, which is well known by the name DPWMMAX. So, in the regard of ADPWM methods DPWMMAX, DPWMMIN can be considered as continual or split clamping sequences with $\gamma = 0°$ or $\gamma = 60°$. The diagrammatic representations of these two DPWM methods are shown in the Fig. 2a and b. Another well-known DPWM method clamps every phase at the start and at the end for a period 30° duration for every 180° of its fundamental voltage. It is popularly called by the name DPWM1. Another accepted method clamps every phase during the middle 30° for every 90° of its fundamental voltage, which is well known by the name DPWM3. DPWM1 uses $\sigma = 0$ for the first half and $\sigma = 1$ in the second half of the sector-I. DPWM3 employs the reverse.

So change in the zero state is made at the middle of every sector in the case of the DPWM1 and DPWM3 and is pictorially represented in Fig. 3b and c. If the change in the zero state is made at any spatial angle $\alpha = \gamma$, where γ is between 0° and 60° as shown in Fig. 4a, each phase is clamped continually for a period of 60°, whereas if it is as shown in Fig. 4b, each phase clamps for a period of 60° but the clamping period splits into two parts one with a width of γ in the first quarter and other with a width of $(60° - \gamma)$ in the next quarter in every half cycle. These techniques are termed as "continual clamping" and "split clamping" techniques, respectively, [17]. Here onwards, DPWM1 and DPWM3 will be referred as continual and split clamping methods with the specified value of γ. The modulating waveforms of both continual and split clamping techniques for $\gamma = 45°$ are illustrated in the Figs. 5 and 6.

Applying the sequence with $\sigma = 0$ in the odd sectors and the sequence with $\sigma = 1$ in the even sectors results in DPW M2, and is diagrammatically represented in the Fig. 3d. Reversal of the sequences as shown in Fig. 3f generates DPWM0 [13]. The modulating waveforms illustrating these are shown in Fig. 2d and f, respectively.

Summarizing this, the constant variable σ can be applied at any spatial angle γ to yield different DPWM methods and when $\gamma \neq 30°$ it results in ADPWM methods and is termed as continual or split clamping method with specified γ.

3 Analysis of ADPWM sequences

3.1 Analysis of stator flux ripple

According to space vector algorithm the reference voltage vector is synthesized in an average sense over a sampling

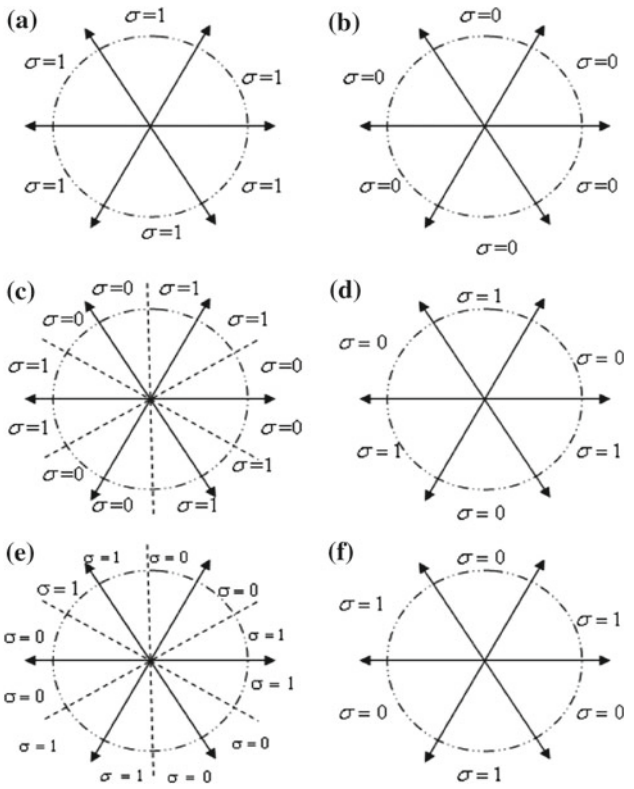

Fig. 3 Generation of space vector-based existing DPWM methods. **a** DPWMMIN, **b** DPWMMAX, **c** DPWM1, **d** DPWM2, **e** DPWM3 and **f** DPWM0

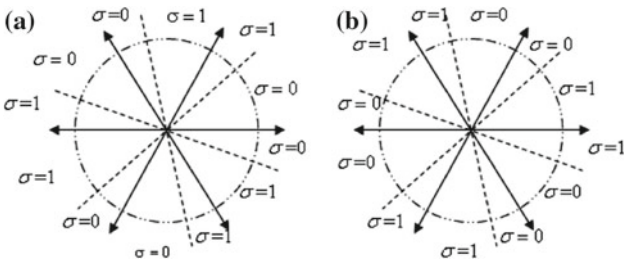

Fig. 4 Generation of space vector-based ADPWM techniques. **a** Continual clamping and **b** split clamping

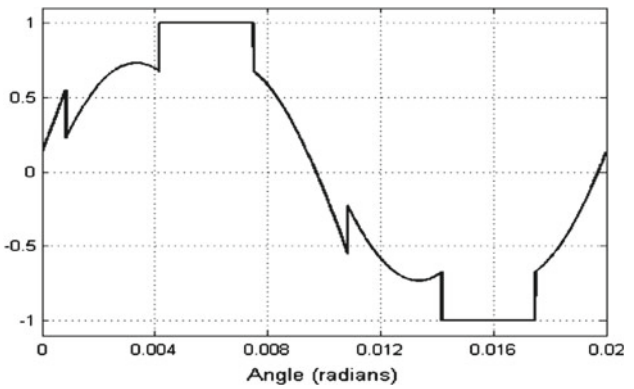

Fig. 5 Modulating waveforms of continual clamping with $\gamma = 45°$

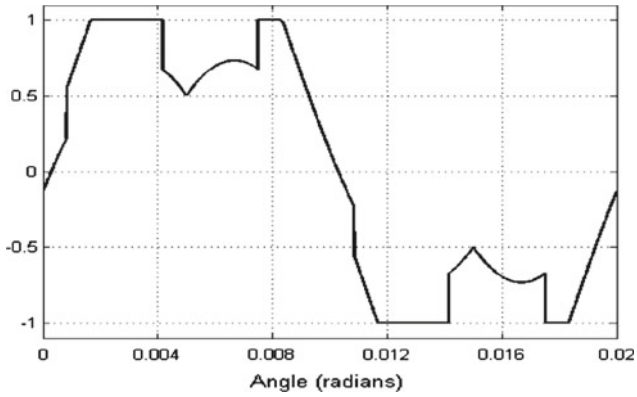

Fig. 6 Modulating waveforms of split clamping with $\gamma = 45°$

period and not instantaneously. The difference between the reference voltage vector and the applied voltage vector is the instantaneous ripple vector.

As the reference voltage vector rotates at synchronous speed, the instantaneous ripple vector changes its magnitude and direction. Resolving the ripple vector in a synchronously rotating $d-q$ reference frame corresponding to the two active states and two zero states gives Q_1, Q_2, Q_Z, D defined as in (4.1–4.4). V_{REF} and α are assumed to be the same for all the sequences, but the carrier cycle duration is T_s for CSVPWM whereas it is $\frac{2T_s}{3}$ for the sequences with $\sigma = 1$ and $\sigma = 0$. Neglecting the stator ohmic drop time integral of the instantaneous ripple is proportional to the stator flux ripple and is a measure of ripple in line current [18]. The d and q axis components of the stator flux ripple over a switching period corresponding to the CSVPWM and the sequences with $\sigma = 1$ and $\sigma = 0$ are shown in Fig. 7.

$$Q_1 = \left[\frac{2}{3}V_{dc}\cos\alpha - V_{\text{REF}}\right]T_1 \tag{4.1}$$

$$Q_2 = \left[\frac{2}{3}V_{dc}\cos(60° - \alpha) - V_{\text{REF}}\right]T_2 \tag{4.2}$$

$$Q_Z = -V_{\text{REF}}T_Z \tag{4.3}$$

$$D = \left[\frac{2}{3}V_{dc}\sin\alpha\right]T_1 \tag{4.4}$$

The RMS stator flux ripple over a sub cycle for the sequences CSVPWM, $\sigma = 1$, $\sigma = 0$, continual clamping with $\gamma = 30°$, split clamping with are denoted by F^2_{CSVPWM}, $F^2_{\sigma=0}$, $F^2_{\sigma=1}$, $F^2_{\text{CONT}}(\sigma = 30°)$, $F^2_{\text{SPLIT}}(\sigma = 30°)$, respectively, and are expressed as in (5.1–5.5). Figure 8 shows the variation of RMS stator flux ripple of the considered existing DPWM methods as well as ADPWM methods over a sector.

$$F^2_{\text{CSVPWM}} = \frac{1}{3}(0.5Q_Z)^2\frac{T_z}{2T_S} + \frac{1}{3}\begin{bmatrix}(0.5Q_Z)^2 \\ +0.5Q_Z(0.5Q_Z + Q_1) \\ +(0.5Q_Z + Q_1)^2\end{bmatrix}\frac{T_1}{T_S}$$

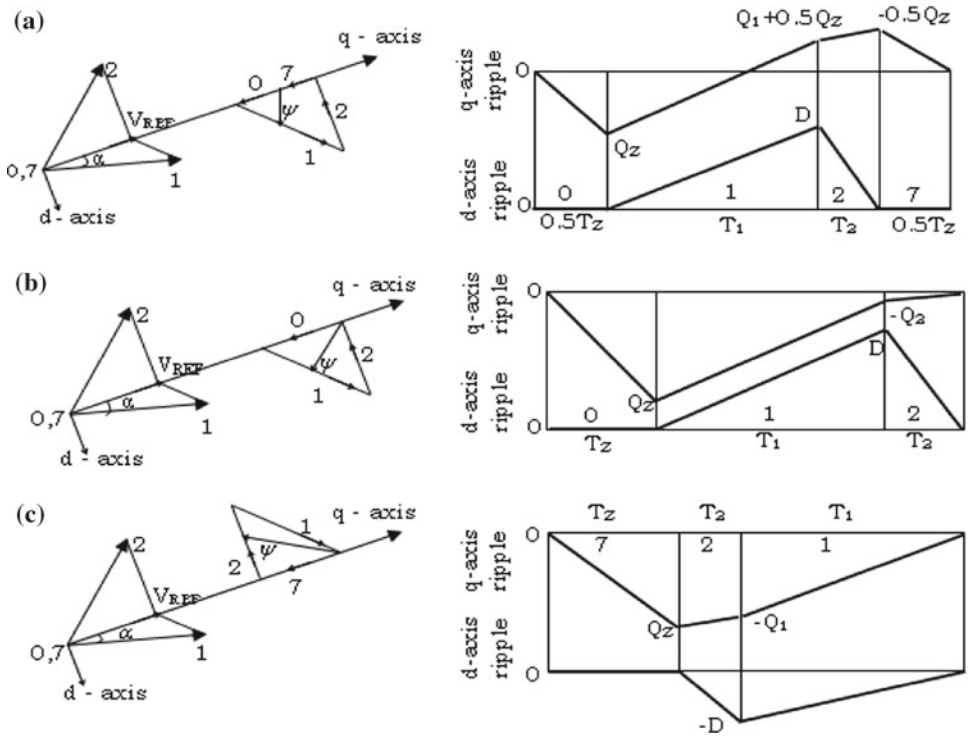

Fig. 7 Stator flux ripple over a sub-cycle and its components along d and q axes corresponding to sequences. **a** CSVPWM, **b** $\sigma = 0$ and **c** $\sigma = 1$

$$+\frac{1}{3}\begin{bmatrix}(0.5Q_Z+Q_1)^2\\-(0.5Q_Z+Q_1)(0.5Q_Z)\\+(-0.5Q_Z)^2\end{bmatrix}\frac{T_2}{T_S}+\frac{1}{3}(-0.5Q_Z)^2\frac{T_Z}{2T_S}+\frac{4}{27}D^2\frac{(T_1+T_2)}{T_S} \tag{5.1}$$

$$F^2_{\sigma=0}=\frac{4}{27}Q_Z^2\frac{T_Z}{2T_S}+\frac{4}{27}\begin{bmatrix}Q_Z^2\\+Q_Z(Q_Z+Q_2)\\+(Q_Z+Q_2)^2\end{bmatrix}\frac{T_2}{T_S}+\frac{4}{27}(Q_Z+Q_2)^2\frac{T_1}{T_S}+\frac{4}{27}D^2\frac{(T_1+T_2)}{T_S} \tag{5.2}$$

$$F^2_{\sigma=1}=\frac{4}{27}Q_Z^2\frac{T_Z}{2T_S}+\frac{4}{27}\begin{bmatrix}Q_Z^2\\+Q_Z(Q_Z+Q_1)\\+(Q_Z+Q_1)^2\end{bmatrix}\frac{T_1}{T_S}+\frac{4}{27}(Q_Z+Q_1)^2\frac{T_2}{T_S}+\frac{4}{27}D^2\frac{(T_1+T_2)}{T_S} \tag{5.3}$$

$$F^2_{\mathrm{CONT}}=F^2_{721},\quad 0^\circ<\alpha\le\gamma \qquad +F^2_{012},\quad \gamma<\alpha\le 60^\circ \tag{5.4}$$

$$F^2_{\mathrm{SPLIT}}=F^2_{012},\quad 0^\circ<\alpha\le\gamma \qquad +F^2_{721},\quad \gamma<\alpha\le 60^\circ \tag{5.5}$$

Observations from Fig. 8 leads to a conclusion that at high modulation indices the sequence that gives minimum ripple will be executed almost through out the sector in the case split clamping DPWM method with $\gamma = 30^\circ$ whereas the sequence that gives high ripple is executed through out the sector in the case of continual clamping DPWM method with $\gamma = 30^\circ$.

3.2 Analysis of harmonic distortion factor

The RMS harmonic distortion factor (HDF) as a function of reference voltage and frequency is given by Eq. (6) where F^2_{seq} is the RMS stator flux ripple of a particular sequence.

$$F_{\mathrm{DF}}=\frac{2\Pi f_1}{V_{\mathrm{REF}}}\sqrt{\frac{3}{\Pi}\int_0^{\frac{\Pi}{3}}F^2_{\mathrm{seq}}\mathrm{d}\alpha}. \tag{6}$$

The harmonic distortion factor of continual and split clamping sequences assuming $\gamma = 30^\circ$ can be calculated using Eq.(7.1, 7.2) [16,17].

$$F_{\mathrm{DF(CONT},\gamma=30^\circ)}=\frac{2\Pi f_1}{V_{\mathrm{REF}}}\sqrt{\frac{3}{\Pi}\left(\int_0^{\frac{\Pi}{6}}F^2_{721}+\int_{\frac{\Pi}{6}}^{\frac{\Pi}{3}}F^2_{012}\right)\mathrm{d}\alpha} \tag{7.1}$$

$$F_{\mathrm{DF(SPLIT},\gamma=30^\circ)}=\frac{2\Pi f_1}{V_{\mathrm{REF}}}\sqrt{\frac{3}{\Pi}\left(\int_0^{\frac{\Pi}{6}}F^2_{012}+\int_{\frac{\Pi}{6}}^{\frac{\Pi}{3}}F^2_{721}\right)\mathrm{d}\alpha} \tag{7.2}$$

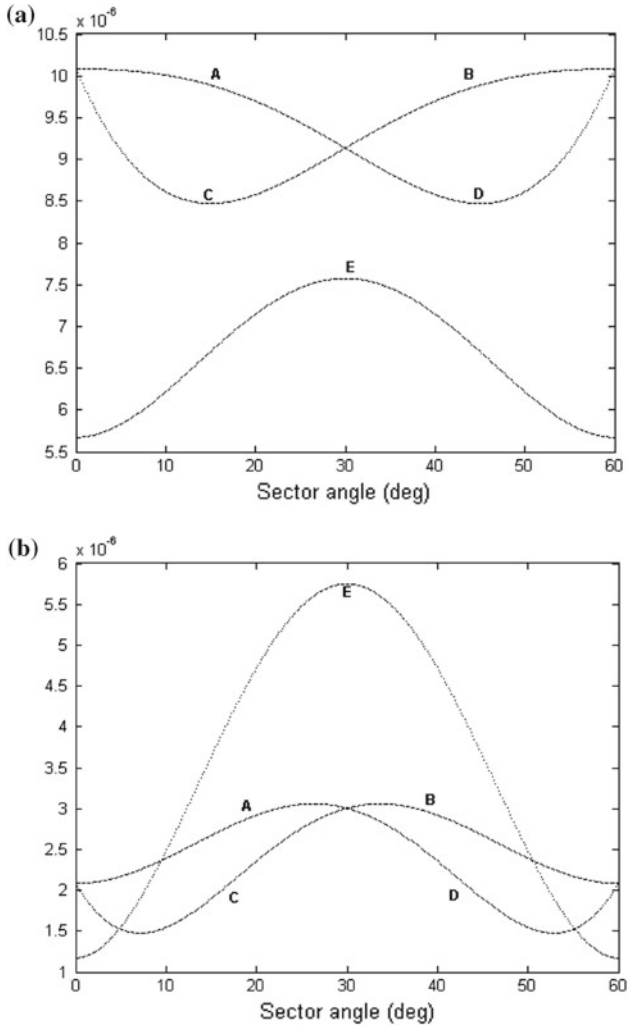

Fig. 8 **a** RMS stator flux ripple within a sector for: *a* AB-continual clamping sequence with $\gamma = 30°$, *b* CD-split clamping sequence with $\gamma = 30°$, *c* AD-DPWMMAX, DPWM2, *d* CB-DPWMMIN, DPWM0, *e* E-CSVPWM at $M = 0.45$. **b** RMS stator flux ripple within a sector for: *a* AB-continual clamping sequence with $\gamma = 30°$, *b* CD-split clamping sequence with $\gamma = 30°$, *c* AD-DPWMMAX, DPWM2, *d* CB-DPWMMIN, DPWM0, *e* E-CSVPWM at $M = 0.75$

Generalizing this HDF of continual clamping or split clamping sequences for which zero vector is varied at any spatial angle γ is given by Eq. (7.1, 7.2).

$$F_{\mathrm{DF(CONT)}} = \frac{2\Pi f_1}{V_{\mathrm{REF}}} \sqrt{\frac{3}{\Pi}\left(\int_0^{\gamma} F_{721}^2 + \int_{\gamma}^{\frac{\Pi}{3}} F_{012}^2\right)} \mathrm{d}\alpha \qquad (7.3)$$

$$F_{\mathrm{DF(SPLIT)}} = \frac{2\Pi f_1}{V_{\mathrm{REF}}} \sqrt{\frac{3}{\Pi}\left(\int_0^{\gamma} F_{012}^2 + \int_{\gamma}^{\frac{\Pi}{3}} F_{721}^2\right)} \mathrm{d}\alpha \qquad (7.4)$$

Since RMS harmonic distortion factor is proportional to the RMS stator flux ripple over a sector, split clamping gives less

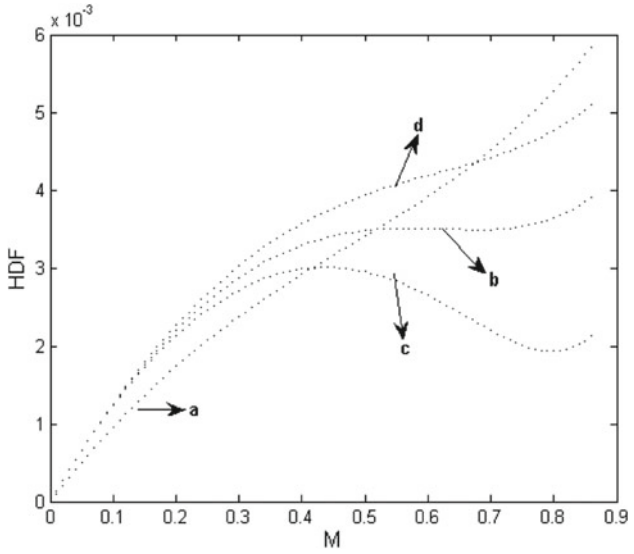

Fig. 9 Analytical evaluation of HDF against modulation index at switching frequency of 5 KHz, $\alpha = 30°$. *a* CSVPWM, *b* continual or split clamping with or $\gamma = 0°$ or $\gamma = 60°$ (DPWMMAX, DPWMMIN, DPWM0, DPWM2), *c* spit clamping sequence with $\gamma = 30°$, *d* continual clamping with $\gamma = 30°$

or equal distortion when compared with continual clamping at all modulation indices and lowest distortion compared with all PWM methods particularly at high modulation indices. Continual or split clamping with $\gamma = 0°$ or $\gamma = 60°$ gives same distortion because in these two methods for half of the sector the sequence that gives minimum ripple will be executed and for the other half sequence that gives highest ripple will be executed. The same thing holds good for DPWM0, DPWM2. The intersection of a particular DPWM method with SVPWM defines the optimal transition point. Although at high modulation indices split clamping method with $\gamma = 30°$ gives least HDF the movement is limited between curves '*c*' and '*d*', determined by the value of γ. This is established from the Fig. 9.

4 Proposed DTC IM drive

The block diagram of the proposed ADPWM-based DTC is shown in the Fig. 10. With the proposed method ripples in torque and flux at high modulation indices are reduced significantly maintaining constant switching frequency. The proposed DTC retains all the advantages of the CDTC, in addition to this gives enhanced performance in high modulation regions which is a limitation with CSVPWM-based DTC.

Addition of slip speed to the actual speed generated by the adaptive motor model block generates reference stator flux vector. The reference *d* and *q* axis voltages are calculated by the reference voltage vector calculator using Eq. (6). Taking

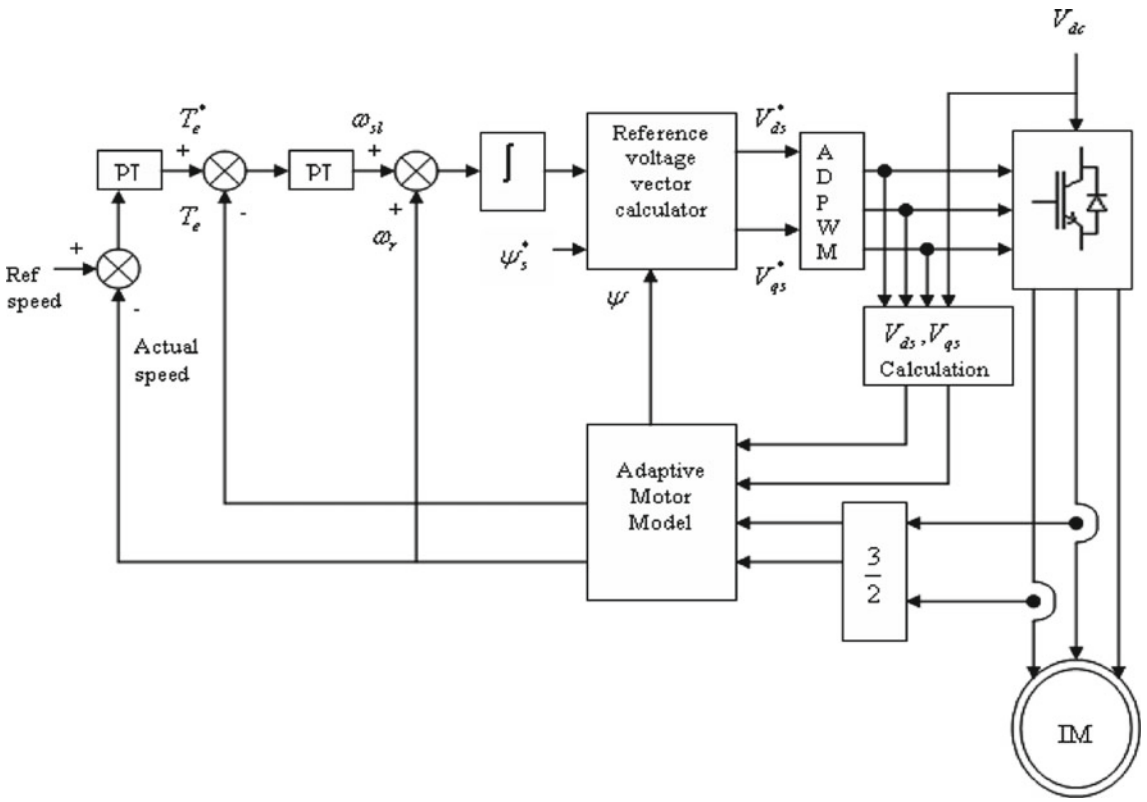

Fig. 10 Block diagram of the proposed ADPWM-based DTC

these two as inputs the magnitude and position of the reference voltage vector are calculated and according to the set value of γ. The ADPWM block generates gating pulses to the inverter based on space vector approach. The adaptive motor model estimates the torque and speed from the d and q axis voltages and currents. The dynamic model of the induction motor is modeled in stationary reference frame.

$$V_{ds}^* = R_s i_{ds} + \frac{\Delta\psi_{ds}}{T_s} \tag{8.1}$$

$$V_{qs}^* = R_s i_{qs} + \frac{\Delta\psi_{qs}}{T_s} \tag{8.2}$$

where

$$\Delta\psi_{ds} = \psi_{ds}^* - \psi_{ds} \tag{8.3}$$

$$\Delta\psi_{qs} = \psi_{qs}^* - \psi_{qs} \tag{8.4}$$

5 Simulation results and discusssion

Simulation was done on V/f controlled induction motor drive in Matlab/Simulink environment. From the tabulated results shown in Table 1, it is observed that compared with CSVPWM both continual and split clamping sequences operating at any spatial angle γ results less ripples in high modulation regions. Among the continual and split clamping sequences continual clamping executes the sequence that gives highest ripple throughout the sector, whereas the split clamping executes the best sequence in terms of ripple through out the sector. For this reason the no-load current ripple due to continual clamping varies directly with $(60^\circ - \gamma)$, whereas no-load current ripple due to split varies inversely with $(60^\circ - \gamma)$. So, compared with CSVPWM reduction in stator current ripple can be achieved with split clamping PWM technique, and analytically it is verified that for $\gamma = 30^\circ$, split clamping gives minimum distortion and hence this method is proposed as optimal ADPWM method.

Simulation results of the proposed ADPWM-based DTC induction drive taking into consideration the different conditions of the drive are presented in Fig. 11. Figure 11a shows

Table 1 Comparison of %THDs of PWM methods for different γ

PWM method	$M = 0.866$
CSVPWM sequence	5.54
Continual clamping sequence with $\gamma = 30^\circ$	5.10
Continual clamping sequence with $\gamma = 45^\circ$	5.03
Split clamping sequence with $\gamma = 30^\circ$	**4.61**
Split clamping sequence with $\gamma = 45^\circ$	4.78

Bold value indicates that the split clamping sequence with $\gamma = 30^\circ$ gives lowest % THD than other PWM methods

the starting transients in three-phase stator currents, torque, speed and stator flux and Fig. 11b shows the no-load steady state ripples. The starting torque is limited to 150% of the rated (15.8 Nm). Figure 11c shows the no-load current and its harmonic spectra. Figure 11d shows the transients during step change in load and Fig. 11e shows the transients during speed reversal. Figures 12a and 13a show the no-load steady state ripples in three-phase stator currents, torque, speed and stator flux of the CDTC, CSVPWM-based DTC induction motor drive. Measured no-load steady state current waveform and its harmonic spectra for CDTC, CSVPWM-based DTC drive are shown in Figs. 12b and 13b, respectively. It is observed that with the proposed method %THD in line current is reduced significantly.

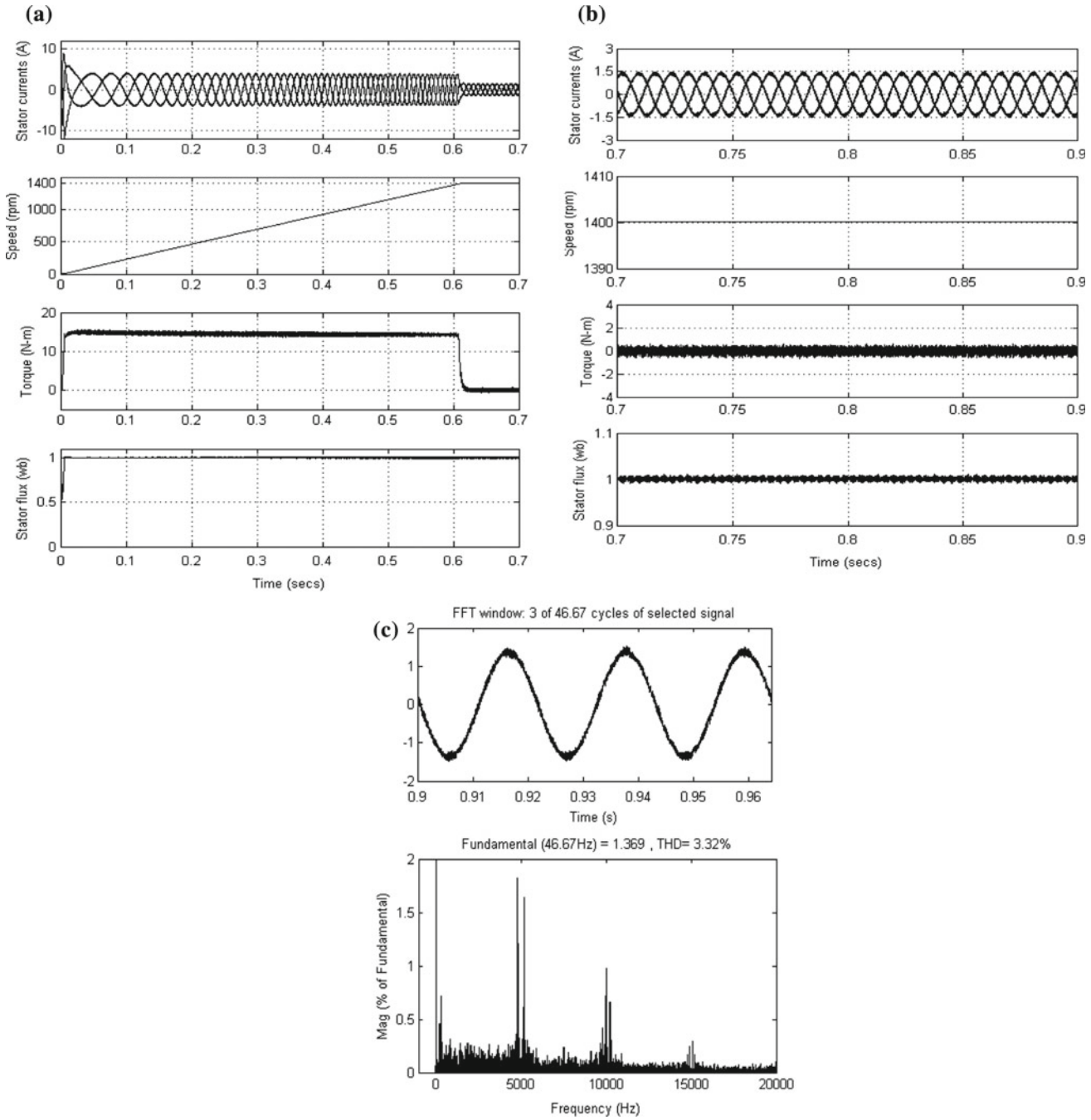

Fig. 11 **a** Proposed ADPWM based DTC: no-load starting transients. **b** Proposed ADPWM-based DTC: steady state ripples **c** split clamping sequence based DTC (with $\gamma = 30°$): measured no-load current and harmonic spectra (% of fundamental). **d** Proposed ADPWM-based DTC: transients during step change in load (a load of 10 Nm is applied at 1 s and removed at 1.4 s). **e** Proposed ADPWM-based DTC: transients during reversal of speed (speed reversal command is given at 1.8 s to change the speed from +1,300 rpm to −1,300 rpm)

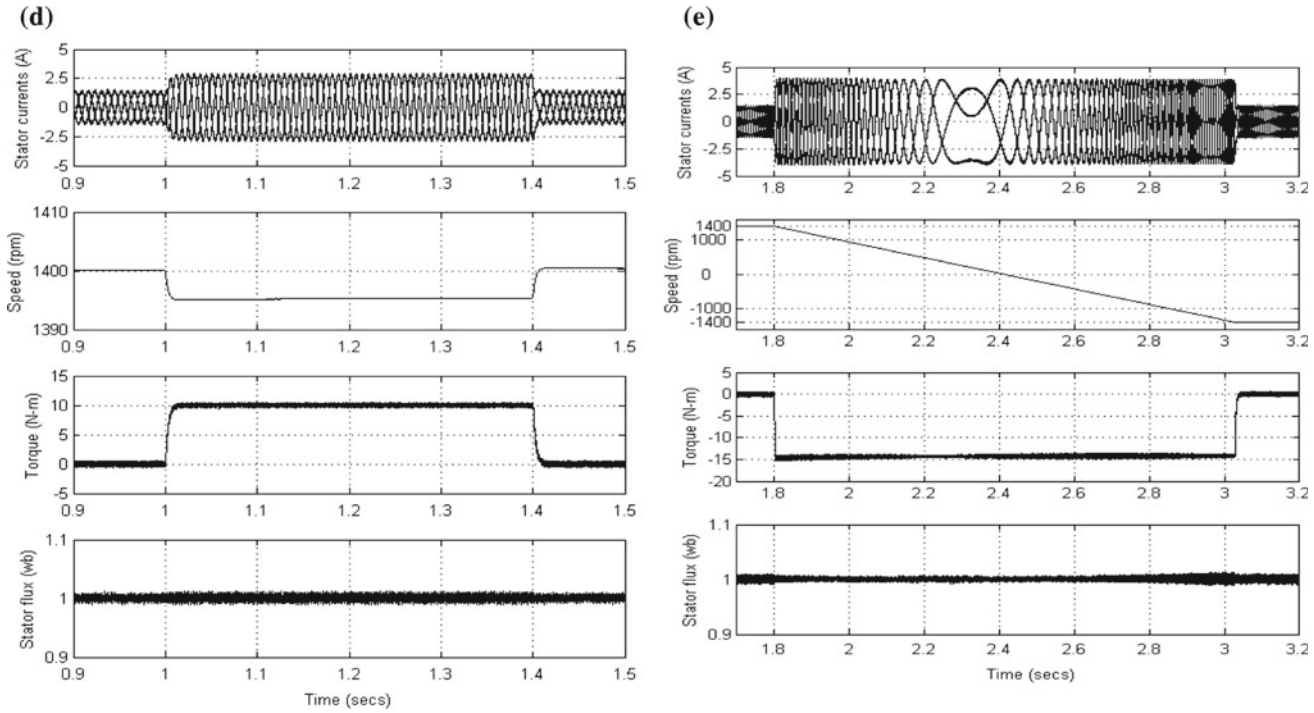

Fig. 11 continued

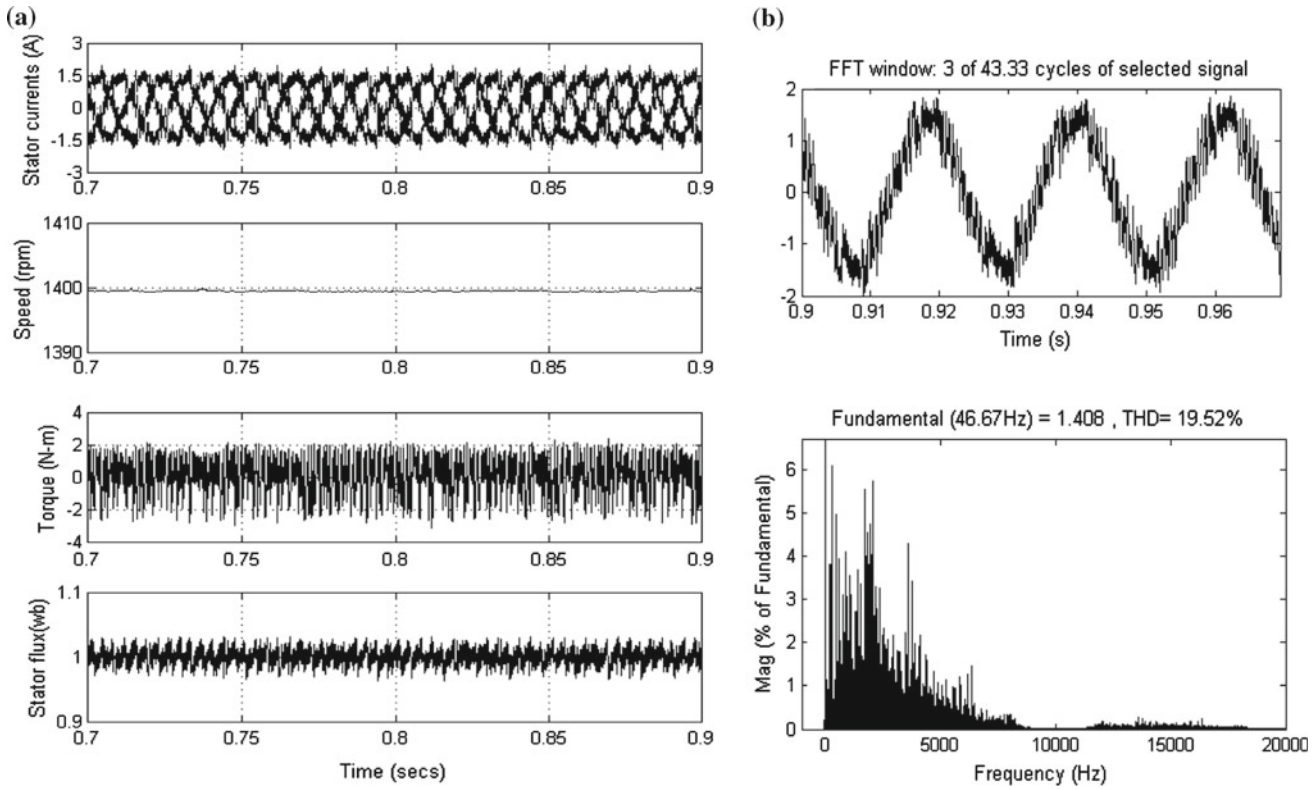

Fig. 12 **a** CDTC: steady state ripples, **b** CDTC: measured no-load steady state current and harmonic spectra (% of fundamental)

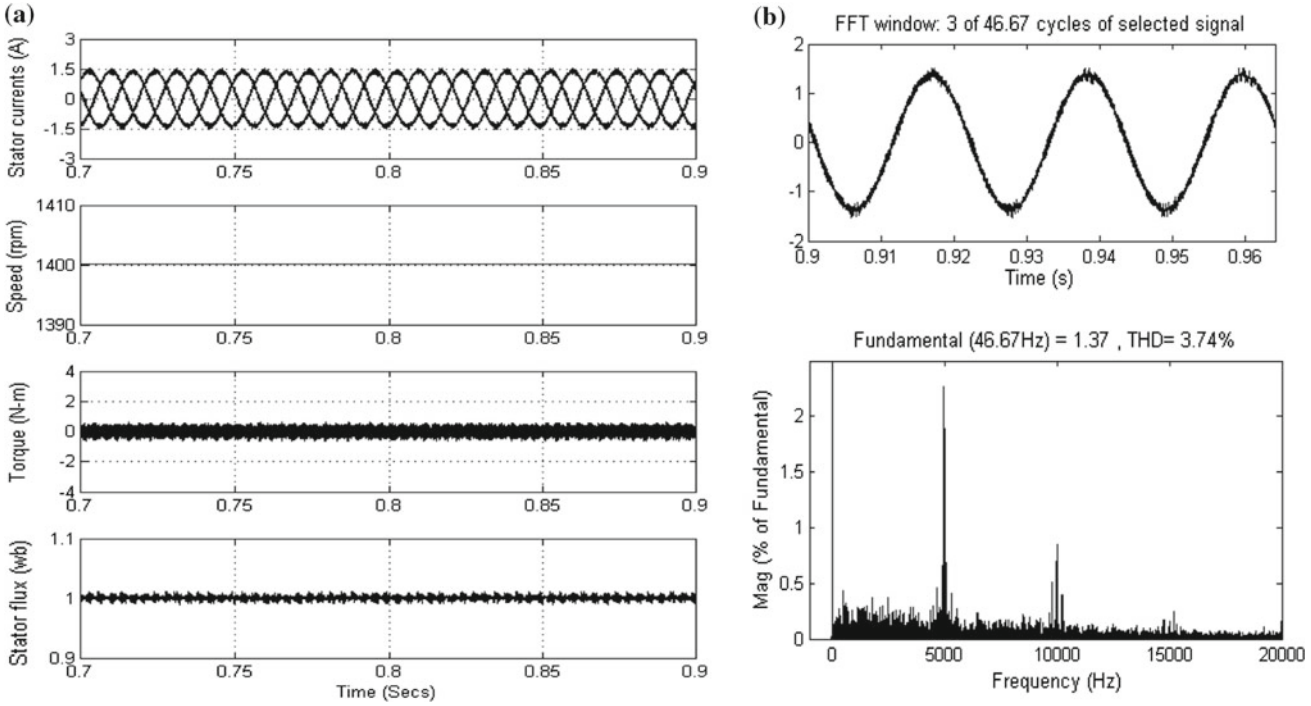

Fig. 13 **a** CSVPWM-based DTC: steady state ripples. **b** SVPWM-based DTC: measured no-load steady state current and harmonic spectra (% of fundamental)

6 Conclusions

CDTC, though simple, because of the limitations like steady state ripple in torque and flux, variable switching frequency, search for PWM technique that gives proper solution is one of the fascinating areas for researchers. SVPWM-based DTC gave answer to some tribulations and now the search is to reduce the ripple in line current particularly in high modulation regions. In this paper, an optimal ADPWM-based DTC induction motor drive is proposed which can exercise a particular value of γ or might select according to a set policy. It is shown that split clamping gives minimum ripple than with continual as well as CSVPWM in high modulation regions. Since split clamping with $\gamma = 30^\circ$ gives minimum ripple, referred as an optimal ADPWM method is proposed for the drive operating at high line side voltages. Simulation results conclude that with the proposed PWM method ripple in steady state line current is reduced significantly when compared with CDTC and CSVPWM-based DTC and so reduced acoustic noise is a distinctive facet of the proposed method. Also, with the proposed method switching losses are reduced when compared with the CSVPWM-based DTC.

References

1. Blaschke F (1972) The principle of field orientation as applied to the new TRANSVECTOR closed loop control system for rotating field machines. Siemens Rev XXXIX 5:217–220
2. Takahashi I, Noguchi T (1986) A new quick-response and high efficiency control strategy of an induction motor. IEEE Trans Ind Appl IA-22(5):820–827
3. Titinen P, Surandra M (1996) The next generation motor control method, DTC direct torque control. IEEE Proc Power Electron Drives Energy Syst Ind Growth 1:37–43
4. Holtz J (1992) Pulsewidth modulation: a survey. IEEE Trans Ind Electr 39(5):410–420
5. Holtz J (1994) Pulsewidth modulation for electronic power conversion. Proc IEEE 82(8):1194–1214
6. Narayanan G, Ranganathan VT (1999) Synchronized PWM strategies based on space vector approach. Part 1: principles of waveform generation. Proc Inst Electron Eng 146(3):267–275
7. Zhou K, Wang D (2002) Relationship between space-vector modulation and three-phase carrier-based PWM: a comprehensive analysis. IEEE Trans Ind Electron 49(1):186–196
8. Holmes DG, Lipo TA (2003) Pulse width modulation for power converters: principle and practice. Wiley, New York
9. Habetler TG et al (1992) Direct torque control of induction machines using space vector modulation. IEEE Trans Ind Appl 28(5):1045–1053
10. Tang L, Zhong L, Rahman MF, Hu Y (2002) An investigation of a modified direct torque control strategy for flux and torque ripple reduction for induction machine drive system with fixed switching frequency. IEEEIAS, pp 837–844
11. Chung D-W, Kim J-S, Sul S-K (1998) Unified voltage modulation technique for real-time three-phase power conversion. IEEE Trans Ind Appl 34(2):374–380
12. Hava AM, Kerkman RJ, Lipo TA (1998) A high performance generalized discontinuous PWM algorithm. IEEE Trans Ind Appl 34(5):1059–1071
13. Hava AM, Kerkman RJ, Lipo TA (1999) Simple analytical and graphical methods for carrier-based PWM-VSI drives. IEEE Trans Power Electron 4(1):49–61

14. Ojo O (2004) The generalized discontinuous PWM scheme for three-phase voltage source inverters. IEEE Trans Ind Electron 51(6):1280–1289
15. Brahmananda Reddy T, Amarnath J, Subba Rayudu D, Haseeb Khan Md (2006) Generalized discontinuous PWM based direct torque controlled induction motor drive with a sliding mode speed controller. IEEE Proc Power Electron Drives Energy Syst Indu Growth, PEDES'06, New Delhi, India, paper no. 3D-11
16. Narayanan G, Ranganathan VT (2005) Analytical evaluation of harmonic distortion in PWM AC drives using the notion of stator flux ripple. IEEE Trans Power Electron 20(2):466–474
17. Narayanan G, Krishnamurthy HK, Di Zhao, Ayyanar R (2006) Advanced bus-clamping PWM techniques based on space vector approach. IEEE Trans Power Electron 21(4):974–984
18. Brahmananda Reddy T, Amarnath J, Subba Rayudu D (2006) New hybrid SVPWM methods for direct torque controlled induction motor drive for reduced current ripple. IEEE Proc Power Electron Drives Energy Syst Ind Growth, PEDES'06, New Delhi, India, Paper no. 3B-20